Principles of Physical Biochemistry

Kensal E. van Holde

Professor Emeritus of Biochemistry and Biophysics
Department of Biochemistry and Biophysics
Oregon State University

W. Curtis Johnson

Professor Emeritus of Biochemistry and Biophysics
Department of Biochemistry and Biophysics
Oregon State University

P. Shing Ho

Professor of Biochemistry and Biophysics
Department of Biochemistry and Biophysics
Oregon State University

PRENTICE HALL
Upper Saddle River, New Jersey 07458

Library of Congress Cataloging-in-Publication Data
Van Holde, K. E. (Kensal Edward)
Principles of physical biochemistry / Kensal E. van Holde, W. Curtis Johnson, P. Shing Ho.
p. cm.
Includes bibliographical references and index.
ISBN 0-13-720459-0
1. Physical biochemistry. I. Johnson, W. Curtis. II. Ho, Pui Shing. III. Title.
QP517.P49V36 1998
572--dc21 97-46067
CIP

Acquisitions Editor: John Challice
Editorial Assistant: Betsy A. Williams
Executive Managing Editor: Kathleen Schiaparelli
Assistant Managing Editor: Lisa Kinne
Manufacturing Manager: Trudy Pisciotti
Art Director: Jayne Coute
Cover Designer: Joseph Sengotta
Cover Art: Rolando Corujo
Production Supervision/Composition: ETP Harrison

Simon & Schuster / A Viacom Company
Upper Saddle River, New Jersey 07458

Printed in the United States of America

10 9 8 7 6 5 4 3 2 1

ISBN 0-13-720459-0

Prentice-Hall International (UK) Limited, *London*
Prentice-Hall of Australia Pty. Limited, *Sydney*
Prentice-Hall Canada Inc., *Toronto*
Prentice-Hall Hispanoamericana, S.A., *Mexico*
Prentice-Hall of India Private Limited, *New Delhi*
Prentice-Hall of Japan, Inc., *Tokyo*
Simon & Schuster Asia Pte. Ltd., *Singapore*
Editora Prentice-Hall do Brasil, Ltda., *Rio de Janeiro*

5

Methods for the Separation and Characterization of Macromolecules

5.1 GENERAL PRINCIPLES

In the preceding chapters we have discussed the diversity, complexity, and dynamics of macromolecular structure. Now we turn to experimental methods for determining these structures and examining their interactions and transformations.

At present, we possess powerful techniques, X-ray diffraction and NMR, that allow us to determine the structures of some macromolecules in astonishing detail; we will describe these in later chapters. But before we can apply physical methods meaningfully, we must first purify the macromolecule of interest, separating it from the multitude of molecules, both large and small, found in most biochemical preparations. When it is purified we usually begin the analysis by obtaining certain preliminary information about each biopolymer. Before we set out to determine the exact structure of a protein, for example, there are certain simple things that we need to find out:

1. Does the protein exist, under physiological conditions, as a simple polypeptide chain or as an aggregate of several chains?
2. If the latter is the case, are the chains of one or several kinds? What are their approximate molecular weights?
3. What is the *approximate* size and shape of the native protein molecule: Is it a globular or fibrous protein?
4. What is its ionic character: Is it most rich in acidic or basic residues?

This chapter describes a group of techniques that are commonly employed to answer questions like these. These are experimental methods in which molecules are moved by forces acting on them; they can, therefore, be referred to collectively as *transport* processes. The various techniques will separate macromolecules on the basis of mass, size, shape, charge, or some combination of these parameters. Thus, they can also be employed in preparative separation and purification.

Some of the techniques we shall describe, like *sedimentation* and *electrophoresis*, involve transport of macromolecules in solution. The most rigorous analysis of such transport is based on a general theory called *thermodynamics of irreversible processes*; this we will defer until Chapter 14. Here we introduce a simpler, more intuitively comprehensible and usually quite satisfactory analysis that is based on the concept of forces acting on individual molecules. We shall call this the *molecular-mechanics* approach, and use it exclusively in this preliminary treatment.

Taking this mechanical point of view, let us imagine, in a solution, a solute molecule to which an external force F is suddenly applied. An electric field might be switched on or a centrifugal force imposed by spinning the solution. Whatever its previous random motion may have been, the molecule will also now be accelerated by the imposed force. But this acceleration will last for only an *exceedingly* short time (on the order of nanoseconds; see Figure 5.1 and Exercise 5.1), for as its velocity increases, the molecule will experience an increasing frictional resistance to motion through the medium. This frictional force will be given by $-fv$, where v is the velocity and the constant f is called the *frictional coefficient* of the molecule; the minus sign indicates that friction opposes the motion.

A constant velocity will be reached when the total force on the molecule is zero:

$$-fv + F = 0, \text{ or } F = fv \tag{5.1}$$

Thus, if we can measure the velocity of motion produced by a known force, we can determine the frictional coefficient. This is *one* of the reasons for the study of transport processes, for f depends on the size and shape of the molecule.

The frictional resistance arises because solvent must flow *around* the moving object, and energy must therefore be expended because of the viscosity of the fluid. The theory of frictional coefficients is a difficult exercise in hydrodynamics, and exact expressions have been obtained for only a few simple particle shapes. For example, for a sphere of radius R

$$f_0 = 6\pi\eta R \tag{5.2}$$

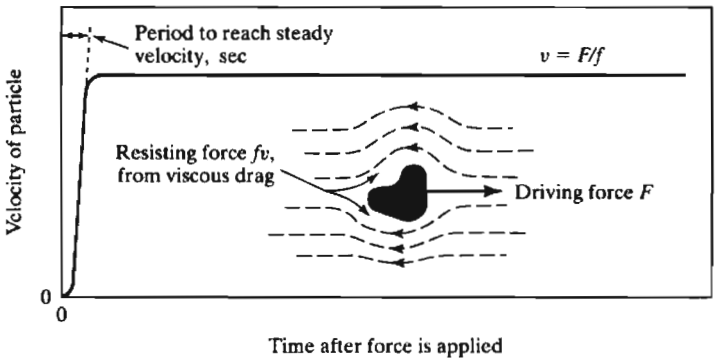

Figure 5.1 A schematic picture of the behavior of a particle suddenly subjected to a force F.

TABLE 5.1 FRICTIONAL COEFFICIENT RATIOS

Shape	f/f_0	R_e
Prolate ellipsoid	$\dfrac{P^{-1/3}(P^2-1)^{1/2}}{\ln[P+(P^2-1)^{1/2}]}$	$(ab^2)^{1/3}$
Oblate ellipsoid	$\dfrac{(P^2-1)^{1/2}}{P^{2/3}\tan^{-1}[(P^2-1)^{1/2}]}$	$(a^2b)^{1/3}$
Long rod	$\dfrac{(2/3)^{1/3}P^{2/3}}{\ln 2P-0.30}$	$\left(\dfrac{3b^2a}{2}\right)^{1/3}$

In these equations, $P = a/b$, where a is the semimajor axis (or the half-length for a rod) and b is the minor axis (or radius of a rod). R_e is the radius of a sphere equal in volume to the ellipsoid or rod, so $f_0 = 6\pi\eta R_e$.

where η is the viscosity of the medium. Eq. 5.2 is called *Stokes' law*. It is found that for a given particle volume, a sphere will have the minimum possible frictional coefficient[1], which we call f_0. Therefore, for any of the other particle models listed in Table 5.1, we list the ratio (f/f_0) between the frictional coefficient of the particle to that of a sphere of equal volume. This *frictional ratio* is always ≥ 1, as shown in Figure 5.2.

Although we shall find this kind of analysis of transport processes to be very useful in subsequent chapters, it must be realized that it is at best an approximate treatment. We cannot always precisely define the force applied to an individual molecule by a known external field, and equations such as Stokes' law have been derived only for the motion of particles through continuous media. The actual chaotic interactions with individual solvent molecules are neglected entirely. However, the approach is sufficiently accurate for large biopolymers that we can confidently use these transport processes in the study of macromolecules. One technique, *mass spectrometry*, which we will discuss in Section 5.4, is free from these approximations. This is because particles being analyzed in a mass spectrograph are moving in a vacuum. This allows unrivaled accuracy in the determination of macromolecular mass by this method.

We now turn to the descriptions of a number of specific techniques, beginning with one familiar in some ways to all biochemists.

5.2 SEDIMENTATION

We shall introduce the concept of sedimentation using the simple mechanical analysis described above, leaving the more mathematically elegant thermodynamic theory for Chapter 14. Imagine a solute molecule in a solution that is held in a rapidly

[1]A good question would be: Why does a "streamlined" teardrop shape not have a lower f? The answer is that molecules are continually tumbling due to random impacts by solvent molecules. The *average* f of a teardrop (which is sometimes going sideways) is higher than that for a sphere of the same volume.

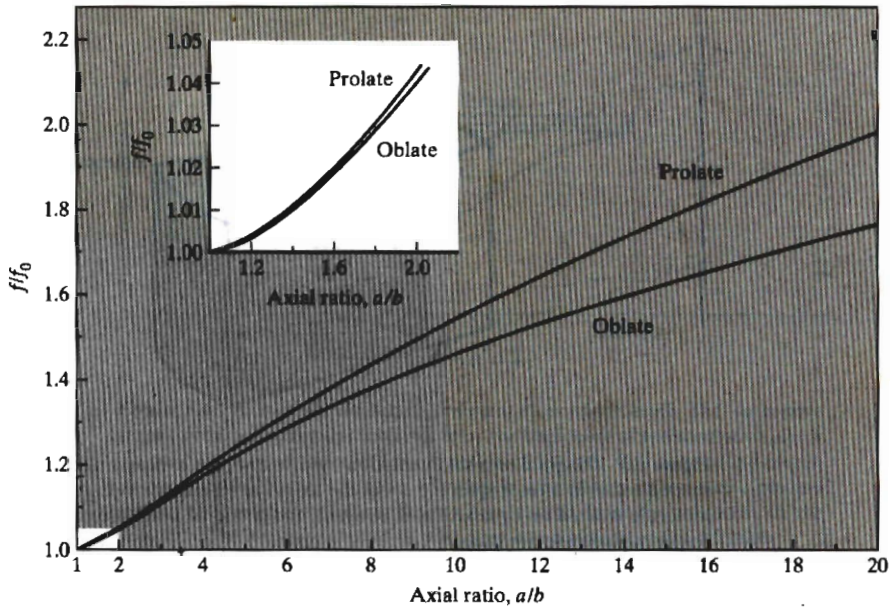

Figure 5.2 The dependence of frictional coefficient on particle shape for ellipsoids. The ratio f/f_0 is the frictional coefficient of a particle of the given axial ratio divided by the frictional coefficient of a sphere of the same volume.

spinning rotor. Forgetting for the moment the random pushes and pulls that the molecule receives from its neighbors, we may say that there are three forces acting on it (see Figure 5.3). If the rotor turns with an angular velocity ω (radians per second) the molecule will experience a *centrifugal* force proportional to the product of its mass (m) and the distance (r) from the center of rotation, $F_c = \omega^2 rm$. At the same time, the molecule displaces some solution and is buoyed up by it; this will give rise to a counter force equal to that which would be exerted on the mass of solution displaced, $F_b = -\omega^2 r m_0$. Finally, if as a result of these forces the molecule acquires a velocity v through the solution, the kind of viscous drag discussed above will be experienced: There will be a *frictional force* $F_d = -fv$, where f is the frictional coefficient. As indicated in the introductory section, this kind of situation will result in the molecule acquiring a velocity just great enough to make the total force zero.

$$F_c + F_b + F_d = 0 \tag{5.3}$$
$$\omega^2 rm - \omega^2 r m_0 - fv = 0$$

For the mass of solution displaced, m_0, we may substitute the product of the particle mass times its partial specific volume[2], times the solution density: $m_0 = m\bar{v}\rho$. Therefore,

$$\omega^2 rm(1 - \bar{v}\rho) - fv = 0 \tag{5.4}$$

[2]The partial specific volume is the effective volume per unit mass of a substance dissolved in solution. See Chapter 13 for a precise definition.

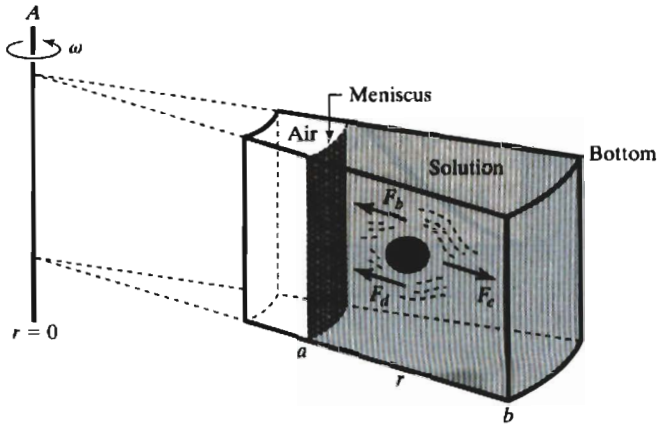

Figure 5.3 Diagram of a sedimentation experiment (not to scale). The sector-shaped cell is in a rotor spinning about the axis A at an angular velocity ω. The molecule is acted on by centrifugal, buoyant, and frictional drag forces. The cell has been given a sector shape because sedimentation proceeds along radial lines; any other shape would lead to concentration accumulation near the edges, with accompanying convection. The angular velocity (ω) is given by ($2\pi/60$) times revolutions per minute.

Next, we multiply Eq. 5.4 by Avogadro's number, to put things on a molar basis, and rearrange, placing the molecular parameters on one side of the equation and the experimentally measured ones on the other.

$$\frac{M(1 - \bar{v}\rho)}{\mathcal{N}f} = \frac{v}{\omega^2 r} = s \tag{5.5}$$

The velocity divided by the centrifugal field strength ($\omega^2 r$) is called the *sedimentation coefficient*, s. According to Eq. 5.5, it is proportional to the molecular weight multiplied by the *buoyancy factor* ($1 - \bar{v}\rho$) and inversely proportional to the frictional coefficient. It is experimentally measurable as the ratio of velocity to field strength. The units of s are seconds. Since values of about 10^{-13} sec are commonly encountered, the quantity 1×10^{-13} sec is called 1 Svedberg, named after T. Svedberg, a pioneer in sedimentation analysis. Svedberg units are conventionally denoted by the symbol S.

5.2.1 Moving Boundary Sedimentation

Determining the Sedimentation Coefficient. What happens when a centrifugal field is applied to a solution of large molecules? Figure 5.4 shows the concentration changes that occur in an ultracentrifuge cell in which the molecules were initially uniformly distributed throughout the solution. When the field is applied, all begin to move, and a region near the meniscus becomes entirely cleared of solute. Thus a *moving boundary* is formed between solvent and solution; this travels down

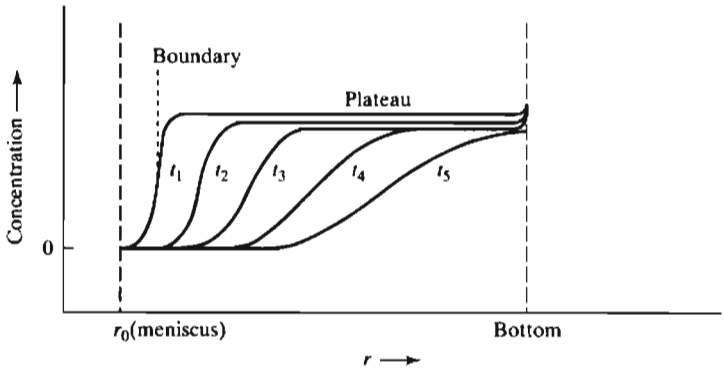

Figure 5.4 A moving boundary sedimentation experiment. The successive graphs, obtained at regular intervals after the beginning of sedimentation, show the concentration of the solute as a function of distance. Cell bottom and meniscus are marked. There is a solute-free region, a boundary region, and a plateau region. The sedimentation coefficient is measured from the midpoint of the boundary. The boundary broadens with time as a consequence of diffusion.

the cell with a velocity determined by the sedimentation velocity of the macromolecules. We can, therefore, measure the sedimentation coefficient by following the rate of this boundary motion; this is what an *analytical ultracentrifuge* is designed to do. A schematic diagram of a modern analytical centrifuge is shown in Figure 5.5. The rotor spins (up to 70,000 rpm) in an evacuated chamber (to reduce friction heating) and its speed and temperature are closely controlled. The progression of sedimentation is observed by a *scanning absorption optical system*. The ultracentrifuge is equipped with a light source and monochromator, so that a wavelength can be selected at which the solute absorbs UV light maximally. The ultracentrifuge cell is illuminated by this light each time it revolves through the optical path. Focusing mirrors are arranged to form a cell image; this image is then scanned by a photomultiplier as it is displaced in the r direction. A double-sector cell is employed so that the photomultiplier alternately observes solution and solvent; thus the whole system acts as a double-beam spectrophotometer. At each point r, the absorbance difference between the solution sector and the reference sector is recorded. The kind of output obtained is shown in Figure 5.4; it is a series of graphs of absorbance versus r at a succession of times in the sedimentation experiment. The boundary position is usually defined as the midpoint of the absorbance step, and can be recorded at successive times during the experiment. Since the velocity of sedimentation v can be set equal to dr_b/dt, we have, from Eq. 5.5,

$$\frac{dr_b}{dt} = r_b\omega^2 s \tag{5.6}$$

Integrating gives

$$\ln [r_b(t)/r_b(t_0)] = \omega^2 s(t - t_0) \tag{5.7}$$

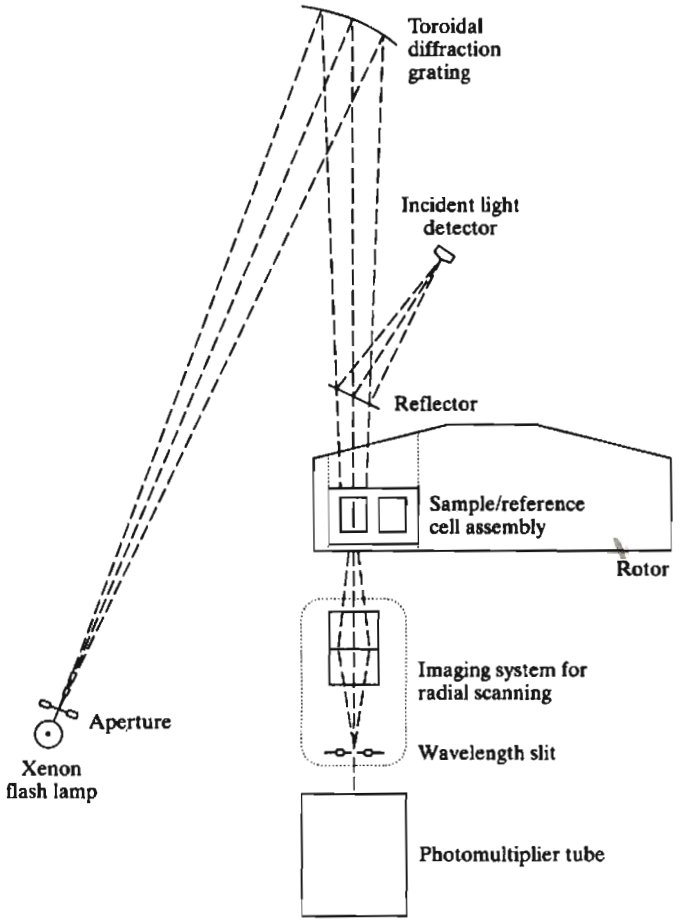

Figure 5.5 A schematic drawing of the absorption optical system for a modern analytical ultracentrifuge. The entire system is contained within the vacuum chamber housing the rotor. The diffraction grating allows choice of monochromatic light from about 200-800 nm. [Courtesy of Beckman Instruments.]

where $r_b(t)$ and $r_b(t_0)$ are positions at t and t_0, respectively. A graph of $\ln r_b(t)$ versus t will be a straight line with slope $\omega^2 s$, which allows us to calculate s.

The boundary does not remain sharp as it moves down the cell. Rather, it broadens because of the phenomenon of *diffusion*. Diffusion is simply another transport process, but one in which molecules are driven in random directions by thermal motion. Diffusion will be described in mechanical terms in Chapter 7; the thermodynamic theory of diffusion will be developed in detail in Chapter 14. For now it will suffice to note that the rate at which the boundary spreads with time is measured by

the *diffusion coefficient*, D. The value of D is proportional to RT (a measure of thermal energy) and is inversely proportional to the frictional coefficient.

$$D = RT/\mathfrak{N}f \tag{5.8}$$

The diffusion coefficient is by convention expressed in cgs units of cm^2/sec. Since D is inversely proportional to f, which in turn depends on molecular size, diffusion will be very slow for large molecules and fast for small ones. This has important effects on sedimenting boundaries. If the diffusion coefficient were zero, the boundary would remain infinitely sharp as it traversed the cell. Such a situation is *approximated* by very large molecules at high rotor speeds. Figures 5.6a,b contrast the behavior of Chambered Nautilus hemocyanin (a) with M = 3,500,000, and its subunit (b) with M = 350,000. In a given length of time the subunit has sedimented only about 1/5 as far, but the boundary has spread much more.

Below the boundary there is always a *plateau* region, which in most cases will extend nearly to the bottom of the cell (see also Figure 5.4). Here the concentration is independent of r and almost (but not quite) the same as the initial concentration. There is a slight radial dilution effect that occurs as sedimentation proceeds (see Chapter 14 for details and explanation). At the bottom of the cell, of course, the solute "piles up" in a dense layer.

The sedimentation coefficient is a characteristic property of each biological macromolecule. However, because it depends on $\bar{v}$, ρ, and f, all of which depend on temperature and the buffer solution in which the molecule is dissolved, it is necessary for comparative purposes to correct values obtained under various experimental conditions to *standard conditions*. These have been chosen to correspond to a hypothetical sedimentation in pure water at 20°C. The variation of f with T and the buffer solutions results entirely from its dependence on viscosity η; see Eq. 5.2. Hence we may write

$$s_{20,w} = s_{T,b}\frac{(1 - \bar{v}\rho)_{20,w}\eta_{T,b}}{(1 - \bar{v}\rho)_{T,b}\eta_{20,w}} \tag{5.9}$$

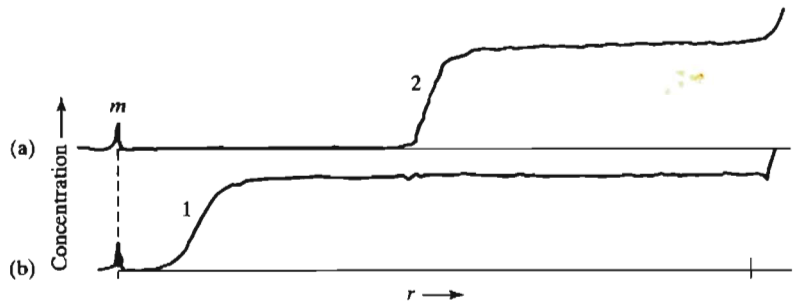

Figure 5.6 Data on (a) sedimentation of Chambered Nautilus hemocyanin ($M = 3.5 \times 10^6$) and (b) hemocyanin subunits at about the same time of sedimentation. Both are homogeneous, but the boundary for the latter has spread much more due to more rapid diffusion.

Here $s_{T,b}$ is the value measured under experimental conditions, and $s_{20,w}$ corresponds to the value expected at the hypothetical standard condition. In practice, we usually do not know the variation of $\bar{v}$ with T and the buffer composition; fortunately, such variation is small in most cases. Furthermore, it is practical to factor the viscosity term into a *relative buffer viscosity* (almost independent of T) and a temperature factor. Then

$$s_{20,w} \cong s_{T,b} \frac{(1 - \bar{v}\rho_{20,w})}{(1 - \bar{v}\rho_{T,b})} \left(\frac{\eta_{T,b}}{\eta_{T,w}}\right)\left(\frac{\eta_{T,w}}{\eta_{20,w}}\right) \tag{5.10}$$

Equation 5.10 allows correction of an observed sedimentation coefficient to standard conditions. Values of ρ and $\eta_{T,b}/\eta_{T,w}$ are available for many buffer solutions, and the variation of water viscosity with temperature is given in Table 5.2.

It is also often important to take into account the fact that s may depend upon macromolecule concentration. Any interaction between the sedimenting molecules will alter the sedimentation behavior. In the most usual case the molecules may be thought of as interfering with one another so as to make the frictional coefficient increase with concentration. If

$$f = f^0(1 + kC + \cdots) \tag{5.11}$$

where f^0 is the value of f at $C = 0$, then

$$s = \frac{s^0}{1 + kC} \tag{5.12}$$

and since k is usually positive, s will decrease with increasing C. As might be expected, this effect is most pronounced with highly extended macromolecules. Figure 5.7 shows representative data for serum albumin (a compact globular protein) and a small RNA. While the two substances have nearly the same s^0, the concentration dependence for the RNA is much greater; this is a common feature of extended molecules like nucleic acids. Fortunately, DNA and RNA absorb ultraviolet light very strongly, allowing us to use very dilute solutions and thereby to escape from these concentration-dependent effects.

TABLE 5.2 DENSITY AND VISCOSITY OF WATER AS A FUNCTION OF TEMPERATURE

T (°C)	ρ (gm/ml)	η (cp)[a]
0.0	1.0004	1.780
5.0	1.004	1.516
10.0	1.0002	1.308
15.0	0.9996	1.140
20.0	0.9988	1.004
25.0	0.9977	0.891
30.0	0.9963	0.7978

[a]Poise are the cgs units of viscosity. Thus, the viscosity of water at 20.0° is 1.004×10^{-2} poise = 1.004 centipoise.

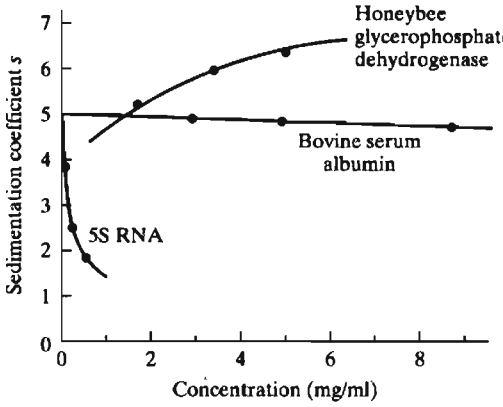

Figure 5.7 Concentration dependence of the sedimentation coefficient. Bovine serum albumin (BSA) and the ribosomal nucleic acid (5S RNA) exhibit behavior typical of compact and extended macromolecules, respectively. The behavior of honeybee glycerophosphate dehydrogenase is that to be expected for a reversibly associating substance. [Data from R. L. Baldwin (1957), *Biochem. J.* **65**, 503; D. G. Comb and Zehavi-Willmer (1967), *J. Mol. Biol.*, **23**, 441; and R. R. Marquardt and R. W. Brosemer (1966), *Biochem. Biophys. Acta*, **128**, 454.]

Also shown in Figure 5.7 are data from a rather different kind of system, in which s *increases* with increasing C (k is negative). In all cases where such behavior has been observed, it appears to result from a rapid monomer-polymer equilibrium. Under some conditions, such systems will yield only a single boundary, with sedimentation coefficient dependent on the proportions of monomer and polymer. Since high concentrations favor polymer formation, the s value increases with C. In any event, it is the sedimentation coefficient extrapolated to zero concentration ($s^0_{20,w}$) that is characteristic of the macromolecule itself. Many such values have been measured; a few are listed in Table 5.3. What can we learn from them?

Interpreting the Sedimentation Coefficient. It is clear from Eq. 5.5 that the sedimentation coefficient will, in general, increase with increasing molecular weight. However, the relationship is not straightforward, for s also depends on f, which in turn depends on the size, shape, and hydration of the macromolecule. Thus, a highly asymmetric molecule might have a lower sedimentation coefficient than a globular protein of lower molecular weight. For example compare the values for catalase and fibrinogen in Table 5.3.

TABLE 5.3 SOME SEDIMENTATION AND DIFFUSION DATA

Substance	$s^0_{20,w} \times 10^{13}$ (sec)	$D^0_{20,w} \times 10^7$ (cm²/sec)	$\bar{v}_{20}$ (cm³/g)	$M_{s,D}$
Lipase	1.14	14.48	0.732	6,667
Lysozyme	1.91	11.20	0.703	14,400
Serum albumin	4.31	5.94	0.734	66,000
Catalase	11.3	4.10	0.730	250,000
Fibrinogen	7.9	2.02	0.706	330,000
Urease	18.6	3.46	0.730	483,000
Hemocyanin (snail)	105.8	1.04	0.727	8,950,000
Bushy stunt virus	132	1.15	0.740	10,700,000

Most of these, and many other data, are listed in G. Fasman (1976).

If macromolecules were both spherical and unhydrated, we could derive a direct relationship between $s^0_{20,w}$ and M. This is because the frictional coefficient for an unhydrated sphere of radius R_0 is given by

$$f_0 = 6\pi\eta R_0 \tag{5.13}$$

and R_0 is in turn related to the molecular weight via the anhydrous molecular volume, V_0.

$$\frac{4}{3}\pi R_0^3 = V_0 = \frac{M\bar{v}}{\mathfrak{N}} \tag{5.14}$$

If we solve Eq. 5.14 for R_0 and insert the result in 5.13, we obtain the following expression for the frictional coefficient of an unhydrated sphere.

$$f_0 = 6\pi\eta(3M\bar{v}/4\pi\mathfrak{N})^{1/3} \tag{5.15}$$

Inserting this result into Eq. 5.5 gives Eq. 5.16.

$$s^0_{20,w} = \frac{M(1-\bar{v}\rho)}{\mathfrak{N}6\pi\eta(3M\bar{v}/4\pi\mathfrak{N})^{1/3}} \tag{5.16a}$$

$$= \frac{M^{2/3}(1-\bar{v}\rho)}{6\pi\eta\mathfrak{N}^{2/3}(3/4\pi)^{1/3}\bar{v}^{1/3}} \tag{5.16b}$$

Here η, $\bar{v}$, and ρ correspond to values in water at 20°C, usually expressed in cgs units. According to Eq. 5.16b, the sedimentation coefficient for unhydrated spherical molecules should be proportional to the 2/3 power of the molecular weight. Indeed, we can rearrange Eq. 5.16b to yield

$$s^* = \frac{s^0_{20,w}\bar{v}^{1/3}}{(1-\bar{v}\rho)} = \frac{M^{2/3}}{6\pi\eta\mathfrak{N}^{2/3}(3/4\pi)^{1/3}} \tag{5.17}$$

We then see that the combination of quantities on the left (which we shall call, for convenience, s^*) should be, for any anhydrous and spherical macromolecule, determined uniquely by its molecular weight. In the log-log plot shown in Figure 5.8, a straight line with a slope of 2/3 is predicted.

It is instructive to plot data for a collection of real proteins on this graph. Note that a large number fall on or close to a line parallel to that predicted by Eq. 5.17. These are the *globular* proteins, and their behavior is explained by the fact that each of them departs not too much from sphericity, and all are hydrated to about the same limited degree. Other proteins, like fibrinogen and myosin, fall far below the line; these are highly asymmetric proteins, which have high frictional coefficients.

While it does not allow us to determine molecular weight unambiguously, Figure 5.8 has certain uses. No real macromolecule could correspond to a point *above or to the left of* the upper line, for that would mean that it had a frictional coefficient less than that predicted for an unhydrated sphere of the same molecular weight. Conversely, this tells us that the upper line marks the *lowest* molecular weight possible for any molecule with a given value of s^*. If we are willing to assume that an

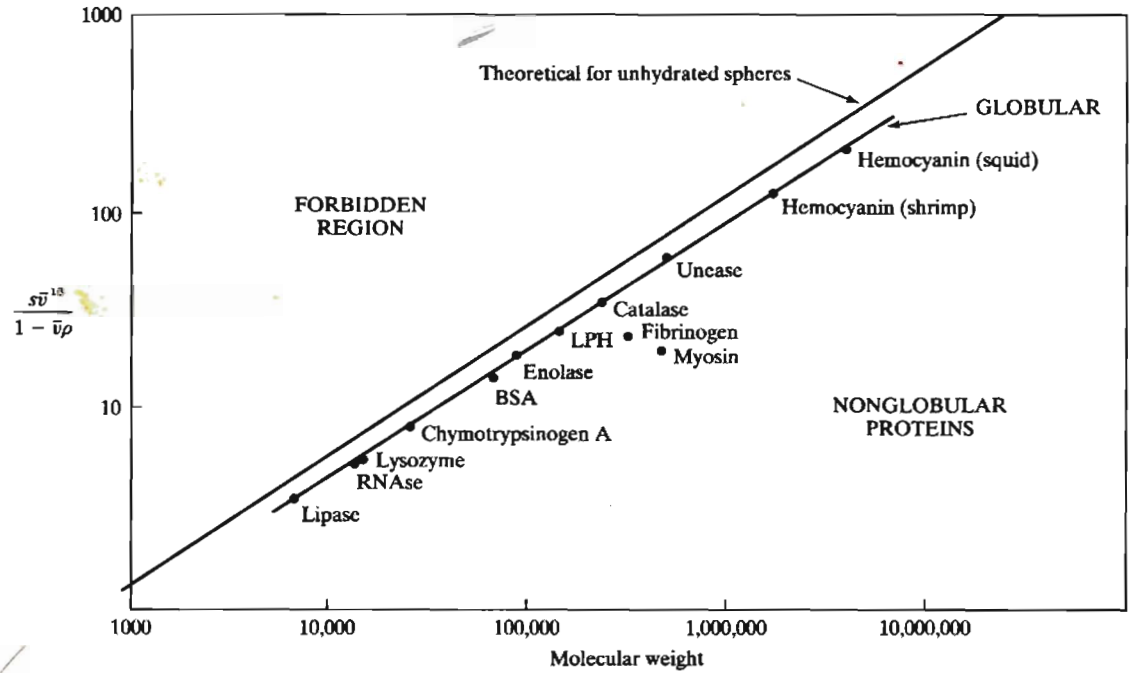

Figure 5.8 Graphs of $s\bar{v}^{1/3}/(1-\bar{v}\rho)$ vs. molecular weight on a log-log scale. The upper line corresponds to Eq. 5.17. Data for various proteins are also plotted on this graph; those for *globular* proteins fall on or close to an empirical line of correct slope (lower line on graph). Note that some *fibrous* proteins deviate markedly from this relationship.

unknown molecule is a typical globular protein, we can use the lower line in Figure 5.8 to estimate M from s^*. But such a procedure can be hazardous; note that if we attempted to use it for the fibrous protein myosin, we would predict a value of $M \cong 100{,}000$, much lower than the correct value of 540,000!

In order to use sedimentation data in this or other ways, it is necessary to know a value for $\bar{v}$. There are two ways to obtain this. The first, which is applicable to all substances, is to measure $\bar{v}$ from solution density measurements. The variation in density for a dilute solution of a molecule of partial specific volume $\bar{v}$ is given to a good approximation by

$$\rho = \rho_0 + (1 - \bar{v}\rho_0)C \tag{5.18}$$

where ρ_0 is the solvent density, and C is the concentration in gm/cm^3. Unfortunately, density measurements of very high precision (on the order of one part in 10^5 or 10^6) are needed to get $\bar{v}$ values good to a few percent at practical biopolymer concentrations. Such measurements are very tedious and difficult. Fortunately, there is a way to circumvent this difficulty, at least for proteins. It has been shown that the $\bar{v}$ of a protein can be quite accurately calculated from its amino acid composition, on the assumption of additivity of *residue volumes*. Tables of such volumes have been developed that yield good results when compared with direct measurement (see Cohn & Edsall, 1943).

If the molecular weight of a macromolecule is known, the sedimentation coefficient can be used to obtain semiquantitative information about its size and shape. As a first approximation, we might calculate the frictional coefficient, f, using a rearranged Eq. 5.5. This then allows us to define an *effective molecular radius*, called the *Stokes radius* (R_s) by

$$f = 6\pi\eta R_s \tag{5.19}$$

However, the significance of this number should not be exaggerated; if the molecule is nonspherical it has no exact physical meaning.

For a slightly more sophisticated analysis, Eq. 5.5 can be used to calculate f, and Eq. 5.15 to calculate f_0. The ratio, f/f_0, will inevitably be somewhat greater than unity. The problem in interpretation comes from the fact that this departure from unity can be accounted for by many possible combinations of different degrees of hydration and different shapes. If we know the hydration from some other kind of measurement, the analysis can be taken a bit further. We can rewrite f/f_0 in terms of f_{sp}, the hypothetical frictional coefficient for a spherical molecule of a given hydration.

$$f/f_0 = (f/f_{sp})(f_{sp}/f_0) \tag{5.20}$$

Thus f_{sp}/f_0 is a factor depending *only* on hydration; it compares a hydrated sphere to an unhydrated one. If we assume that the total volume of a hydrated molecule is simply the sum of the anhydrous volume and the volume of hydrating water, it is easy to show that

$$f_{sp}/f_0 = (1 + \delta)^{1/3} \tag{5.21}$$

where δ is the volume of water of hydration per unit volume of anhydrous macromolecule. The factor f/f_{sp} is then a pure *shape* factor, measuring how much the molecule differs from sphericity. This can be interpreted quantitatively if the shape of the molecule is known. For example, if we know that a given molecule is rod-like, curves like those shown in Figure 5.2 could be used to estimate the length/diameter ratio.

Unfortunately, it has not been possible to deduce *exact* expressions for frictional coefficients for any but the simplest (and often unrealistic) models: spheres, ellipsoids, and the like (see Figure 5.2 and Table 5.1). There exists, however, a theory that allows us to approximate rather accurately the frictional coefficients for molecules of quite complicated shapes. In 1954, J. Kirkwood analyzed the frictional behavior of a molecule made up of a number of subunits, and showed how the hydrodynamic interaction between those subunits could be taken into account. For a particle of N identical subunits, each with frictional coefficient f_1, the frictional coefficient of the assembly can be written as

$$f_N = Nf_1\left(1 + \frac{f_1}{6\pi\eta N}\sum_{i=1}^{N}\sum_{j\neq i}^{N}\frac{1}{R_{ij}}\right)^{-1} \tag{5.22}$$

Here R_{ij} is the distance between subunits i and j, and the summation is taken over all pairs (except $i = j$). This is an exceedingly powerful equation, for in principle it allows us to calculate the frictional coefficient of *any* object by modeling it in terms of a large number of small subunit beads (see Bloomfield et al. 1967). Such calculations are inexact for very asymmetric shapes because of certain approximations in the theory. However, the Kirkwood method is quite useful and practical for the study of multi-subunit proteins. Suppose we have a protein made up of N identical subunits, each with sedimentation coefficient s_1, where

$$s_1 = \frac{M_1(1 - \bar{\nu}\rho)}{\mathcal{N}f_1} \tag{5.23}$$

If we combine Eqs. 5.22 and 5.23, and note that $M_N = NM_1$, we obtain a simple expression for the ratio of the sedimentation coefficient of the N-mer to that of the subunit.

$$\frac{s_N}{s_1} = 1 + \frac{f_1}{6\pi\eta N}\sum_{i=i}^{N}\sum_{j\neq i}^{N}\frac{1}{R_{ij}} \tag{5.24}$$

The ratio s_N/s_1 will depend on the geometry of the molecule, through the subunit-subunit distances R_{ij}. If we write f_1 in Eq. 5.24 as $f_1 = 6\pi\eta R_s$ (where R_s is the Stokes radius of the subunit) the result becomes even simpler.

$$\frac{s_N}{s_1} = 1 + \frac{R_s}{N}\sum_{i=1}^{N}\sum_{j\neq i}^{N}\frac{1}{R_{ij}} \tag{5.25}$$

The Stokes radius, can, of course, be calculated from s_1 and M_1. Eq. 5.25 allows us to test various postulated geometries of subunit arrangement, provided that s_N, s_1, M_1,

TABLE 5.4 PREDICTED SEDIMENTATION COEFFICIENT RATIOS FOR DIFFERENT TETRAMER STRUCTURES

Structure	s_4/s_1
Linear	2.208
Square-planar	2.353
Tetrahedral	2.500

Calculated assuming spherical subunits in contact, Eq. 5.25.

and N are known. Table 5.4 gives examples of predicted values for s_N/s_1 for various possible quaternary arrangements of a tetramer.

Calculation of M from s and D. We have emphasized that the sedimentation coefficient, by itself, cannot yield an unambiguous value for the molecular weight. This is because of the presence in Eq. 5.5 of the frictional coefficient, which depends in complicated ways on size, shape, and hydration. However, it is possible to eliminate f by making use of measurements of the diffusion coefficient. If we divide Eq. 5.5 by Eq. 5.8, we obtain

$$\frac{s}{D} = \frac{M(1 - \bar{v}\rho)/\mathcal{N}f}{RT/\mathcal{N}f} = \frac{M(1 - \bar{v}\rho)}{RT} \tag{5.26}$$

in which s and D must be measured under (or corrected to) the same conditions. Equation 5.26, which has been named the *Svedberg equation*, was one of the first equations used to show that biopolymers are giant molecules. It has been used less frequently recently because of the inconvenience of classical methods for measuring D. However, the development of the fast, accurate laser scattering method (Chapter 7) may make it once again an attractive approach. (Some results from s/D calculations are shown in Table 5.3).

Analysis of Mixtures in Moving Boundary Sedimentation. So far, we have dealt only with sedimentation of a single macromolecular component. If there are multiple components present (as in Figure 5.9), it is often possible to determine both the sedimentation coefficient and amount of each, provided that their boundaries can be resolved. The enemy of resolution is diffusion, which blurs boundaries and makes them overlap. Since boundary spreading due to diffusion proceeds at a rate determined only by the diffusion coefficient of the component concerned, whereas the rate of boundary *separation* depends on the actual velocities of boundary motion, higher rotor speeds will in general lead to greater resolution.

It is possible to compensate for the smearing effect of diffusion by taking advantage of a peculiar difference between sedimentation transport and diffusive transport. The distance traveled by sedimenting molecules is very nearly proportional to the time of sedimentation. However, molecules wandering about in diffusion will, on average, travel distances proportional to the *square root* of time. (See Chapters 4 and 14 for direct demonstrations of this.) This means that as sedimenta-

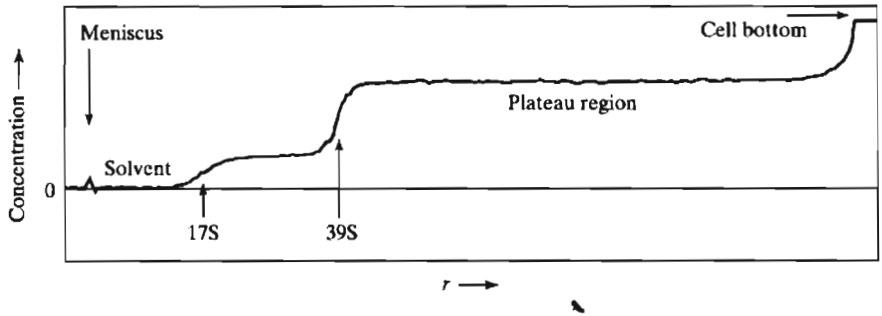

Figure 5.9 The concentration profile expected for a two-component solute that does not show reversible association-dissociation reactions. The amounts of the two components can be approximately calculated from the plateau heights. The data shown are for shrimp hemocyanin.

tion proceeds for longer and longer times, the *separation* between different components becomes more and more dominant over the spreading of any one boundary. van Holde and Weischet (1975) have utilized this fact to extrapolate out the diffusion smearing. Figure 5.10 shows how the diffusion-smeared boundary produced by a single, homogeneous substance can be corrected so as to demonstrate this homogeneity.

Using modern instrumentation and averaging computer-processed data, a quite high precision (of the order of $\pm 1\%$) can be obtained by the moving boundary sedimentation method. Actually, the quantity hardest to obtain with high accuracy is the partial specific volume (see p. 200). Since $\bar{v}$ is approximately 0.7 for most proteins, an error of 1 percent in $\bar{v}$ gives an error of about 3 percent in $(1 - \bar{v}\rho)$ and, consequently, in M.

5.2.2 Zonal Sedimentation

The moving boundary technique, precise as it can be, suffers from a number of disadvantages that have limited its use. First, an expensive and specialized instrument is required. Second, because the recording of concentrations depends primarily on UV absorption, fairly high concentrations (especially for proteins—about 1 mg/ml) are required. Finally, and perhaps most important, the moving boundary technique has difficulty in resolving complex mixtures, since only the *slowest* component is wholly resolved from others. If a narrow *zone* of material could be placed at the meniscus and sedimented through the cell, resolution would be enhanced, for each component would form its own sedimenting zone (see Figure 5.11a). However, a moment's reflection shows that this is not so easy to achieve. Placing a zone containing macromolecules on top of solvent will lead to immediate convection, for the solute-containing zone will be more dense than solvent. However, stable zonal sedimentation can be accomplished if the solution is layered onto a *density gradient* produced by some inert substance (Figure 15.11b). Such a density gradient can be produced using a substance like sucrose or glycerol by carefully layering solutions of

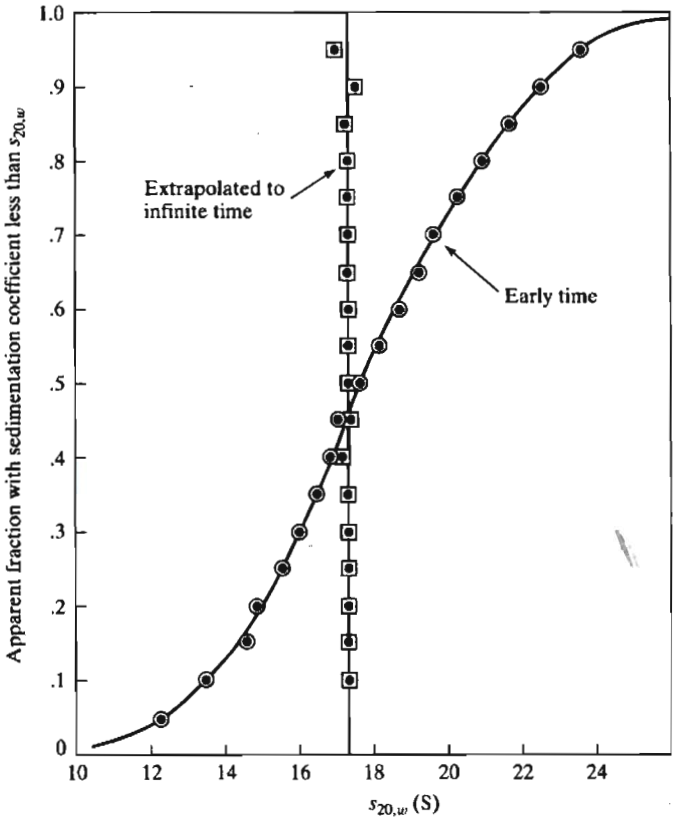

Figure 5.10 Removing the deleterious effect of diffusion smearing on boundary resolution. Data are from a study of squid hemocyanin. The curve with the circles depicts the apparent distribution of sedimentation coefficients at an early time during an experiment. The line through the squares shows the apparent distribution when extrapolated to infinite time. The fact that it is a vertical "step" function shows that the sample is homogeneous, with $s_{20,w} = 17.2\ S$.

decreasing density one upon the other with a mixing device of the kind shown in Figure 5.12; in this way a smooth gradient of any steepness desired can be made. The variation of density with sucrose concentration is shown in Table 5.5.

The gradient produced in this way is, of course, not indefinitely stable; it will eventually disappear by diffusion. But this process is slow, and experiments with a duration of several hours can be performed without too much change occurring in the gradient. The macromolecular solution must be layered onto the gradient with care, and it must be less dense than the top sucrose solution. It is important that the solution layered onto the gradient be not too concentrated and dense. Otherwise the band will be unstable as it moves into the gradient, and resolution will be lost because of localized convection (see Figure 5.13).

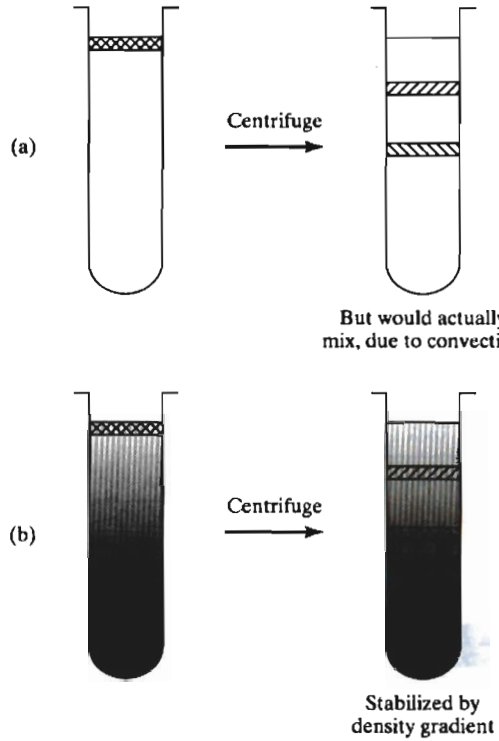

Figure 5.11 The principle of Zonal Sedimentation. (a) The concept of zonal separation. A thin layer containing two different components will separate into two zones after transport. (b) The imposition of a density gradient will allow the zones to be stable against convection.

The advantage in the resolving power of the gradient technique over the conventional sedimentation transport experiment should be obvious. In the conventional method, only the most slowly sedimenting material can be recovered in pure form, whereas the density gradient method completely resolves components from one another. The crude-appearing sampling technique actually works well and little remixing is produced. More sophisticated and reproducible techniques have been developed for emptying the tubes when high precision is needed. From the tube number in which a given component appears, the distance traveled can be estimated and s can be calculated. However, as shown in Table 5.5 the variation in both density and viscosity in the sucrose gradient makes the velocity vary during sedimentation and complicates the calculations. We note that the *velocity* of sedimentation at point r will be given by

$$v = s\omega^2 r = \frac{M(1 - \bar{v}\rho)\omega^2 r}{Nf} \tag{5.29}$$

The frictional coefficient is proportional to η, which increases with r because of the gradient, and $(1 - \bar{v}\rho)$ decreases with r; thus there are two factors that tend to make the velocity become slower and slower as the band moves down the tube. On the other hand, the value of r in Eq. 5.29 is increasing, tending to accelerate the motion.

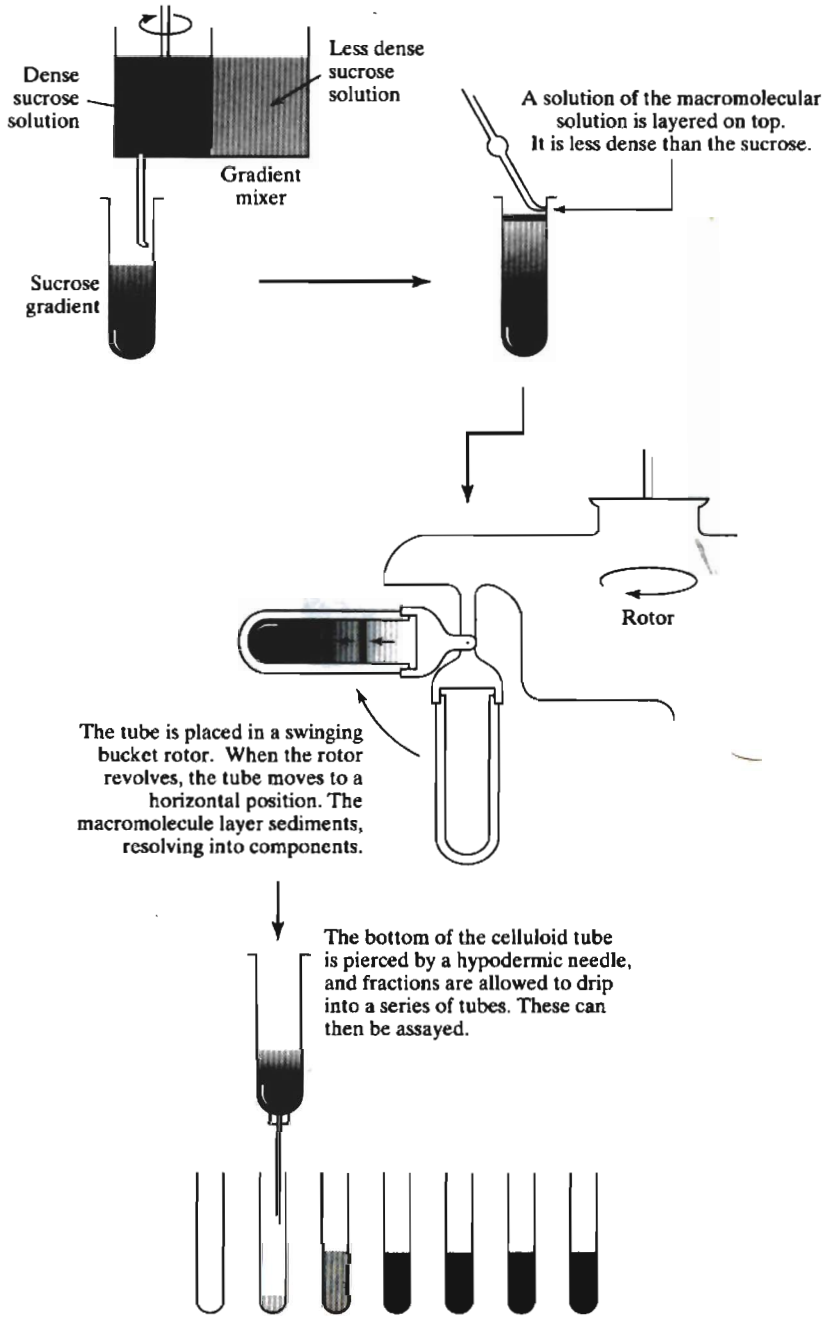

Figure 5.12 Sucrose gradient centrifugation.

TABLE 5.5 DENSITY AND VISCOSITY OF SUCROSE SOLUTIONS AT 20°C

Sucrose (%)	ρ (gm/ml)	η (cp)
0	0.9988	1.004
5	1.0179	1.148
10	1.0380	1.337
15	1.0588	1.592
20	1.0806	1.946
25	1.1033	2.449
30	1.1268	3.189
35	1.1513	4.323
40	1.1766	6.163
45	1.2028	9.376
50	1.2299	15.42
55	1.2578	28.07
60	1.2867	58.50

All data are from more extensive tables in Fasman (1976).

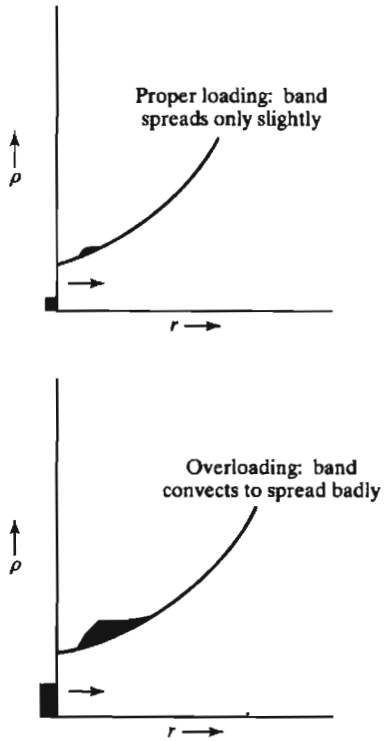

Figure 5.13 The danger in overloading a density gradient experiment. Too concentrated a solution layered on the gradient produces local convection.

If the form of the gradient is chosen correctly, these factors will balance and sedimentation will proceed at a nearly constant rate. The gradient that will produce this effect is called an *isokinetic* gradient, and directions for the construction of isokinetic gradients have been worked out for a number of experimental situations (see, for example, Fasman 1976, Vol. 1, pp. 426–429). Even with an isokinetic gradient, it is advisable to include with the sample two or more marker substances of known sedimentation coefficient to provide an internal calibration scale. With the greatest of care the density gradient method still cannot match the precision of moving boundary sedimentation. Density gradient centrifugation does, however, have the enormous advantage that a wide variety of assay techniques can be used to detect the various components. For example, materials can be specifically labeled with radioactive isotopes or discriminating enzymatic or immunological assays can be used. In this way the sedimentation of a minor component in a crude mixture can be followed, a feat impossible with the optical methods used in most analytical ultracentrifuges. Figure 5.14 shows the sedimentation of an enzyme mixture in a sucrose gradient.

Last, but by no means least, is the fact that density gradient centrifugation, unlike moving boundary sedimentation, is available to almost every biochemistry laboratory. No special instrument is needed—only a swinging bucket rotor of the type shown in Figure 5.12 and a standard preparative ultracentrifuge in which to spin it.

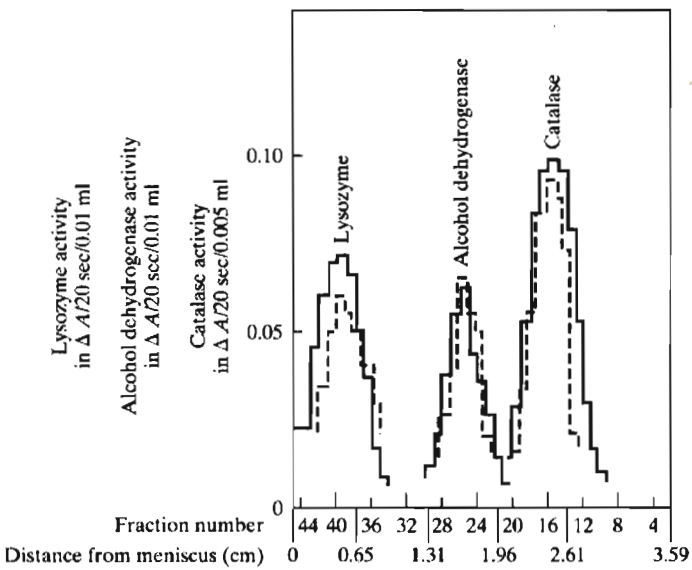

Figure 5.14 A sucrose gradient sedimentation velocity experiment with mixtures of three enzymes. The solid lines show enzyme activities in a mixture of the three enzymes in tris buffer. The dashed lines show activities in a mixture prepared using a crude bacterial extract as the solution medium. In each case, sedimentation was for 12.8 hr at 3°C, 37,700 rpm. [From R. B. Martin and B. Ames (1961), *J. Biol. Chem.*, **236**, 1372.]